Available online at www.sciencedirect.com
ScienceDirect
Journal of Computational Physics 227 (2008) 4190–4206
JOURNAL OF COMPUTATIONAL PHYSICS
www.elsevier.com/locate/jcp

A velocity-estimation subgrid model constrained by subgrid scale dissipation

Noma Park, Krishnan Mahesh *

Department of Aerospace Engineering and Mechanics, University of Minnesota, 110 Union Street SE, Minneapolis, MN 55455, United States

Received 28 February 2007; received in revised form 3 December 2007; accepted 21 December 2007
Available online 2 January 2008

Abstract

Purely dissipative eddy-viscosity subgrid models have proven very successful in large-eddy simulations (LES) at moderate resolution. Simulations at coarse resolutions where the underlying assumption of small-scale universality is not valid, warrant more advanced models. However, non-eddy viscosity models are often unstable due to the lack of sufficient dissipation. This paper proposes a simple modeling approach which incorporates the dissipative nature of existing eddy viscosity models into more physically appealing non-eddy viscosity SGS models. The key idea is to impose the SGS dissipation of the eddy viscosity model as a constraint on the non-eddy viscosity model when determining the coefficients in the non-eddy viscosity model. We propose a new subgrid scale model (RSEM), which is based on estimation of the unresolved velocity field. RSEM is developed in physical space and does not require the use of finer grids to estimate the subgrid velocity field. The model coefficient is determined such that total SGS dissipation matches that from a target SGS model in the mean or least-squares sense. The dynamic Smagorinsky model is used to provide the target dissipation. Results are shown for LES of decaying isotropic turbulence and turbulent channel flow. For isotropic turbulence, RSEM displays some level of backward dissipation, while yielding as good results as the dynamic Smagorinsky model. For channel flow, the results from RSEM are better than those from the dynamic Smagorinsky model for both statistics and instantaneous flow structures.

Keywords: Large eddy simulation; Subgrid scale model; Velocity estimation; Isotropic turbulence; Channel flow

1. Introduction

Despite the impressive growth in available computational resources, the broadband nature of turbulence still hinders the direct numerical simulation (DNS) of all energetic scales at high Reynolds numbers. The small scales are necessarily discarded, and the simulations considered 'under-resolved' at very high Reynolds numbers. Such under-resolved simulations are referred to as large-eddy simulation (LES) when the interactions

* Corresponding author. Tel.: +1 612 624 4175; fax: +1 612 626 1558.
E-mail address: mahesh@aem.umn.edu (K. Mahesh).

0021-9991/$ - see front matter © 2007 Elsevier Inc. All rights reserved.
doi:10.1016/j.jcp.2007.12.020

between resolved and discarded scales are formally modeled. For incompressible flows, LES is governed by the filtered incompressible Navier–Stokes equations:

$$\frac{\partial \bar{u}_i}{\partial t} + \frac{\partial \bar{u}_i \bar{u}_j}{\partial x_j} = -\frac{\partial \bar{p}}{\partial x_i} + \nu \frac{\partial^2 \bar{u}_i}{\partial x_j \partial x_j} - \frac{\partial \tau_{ij}}{\partial x_j}, \tag{1}$$

where $\mathbf{u} = (u_1, u_2, u_3) = (u, v, w)$ denotes the solenoidal Cartesian velocity components, p is the pressure divided by density, ν is the molecular kinematic viscosity, and $\mathbf{x} = (x_1, x_2, x_3) = (x, y, z)$ is the Cartesian position vector. Repeated indices denote summation unless otherwise specified, and the over-bar denotes spatial filtering. For an arbitrary function $\phi(\mathbf{x})$,

$$\bar{\phi}(\mathbf{x}) = \int_\Omega G_\Delta(\mathbf{x}, \mathbf{x}')\phi(\mathbf{x}')d\mathbf{x}', \tag{2}$$

where G_Δ is the kernel of a filter whose nominal size is Δ. In the present study, G_Δ is assumed to be the sharp cut-off filter. Note that we do not consider finite-differencing errors [1], or any explicit filtering [2] other than the grid filter. Also, the nonlinear term is dealiased for all results shown in this paper. The subgrid scale (SGS) stress is defined by $\tau_{ij} = \overline{u_i u_j} - \bar{u}_i \bar{u}_j$ which for the sharp cut-off filter $= \overline{\bar{u}_i u'_j} + \overline{u'_i \bar{u}_j} + \overline{u'_i u'_j}$. Here, $u'_i = u_i - \bar{u}_i$ denotes the SGS velocity components. Note that the term, SGS stress is a little misleading since τ_{ij} is not purely a subgrid scale (SGS) quantity. Although SGS information (u'_i) is required, τ_{ij} is defined on the LES grid. A new SGS model proposed in this paper is partly inspired by this simple observation.

Arguably, the most popular SGS models in practical LES are eddy viscosity models of the form, $\tau_{ij} - \frac{1}{3}\tau_{kk}\delta_{ij} = -2\nu_T(\mathbf{x})\bar{S}_{ij}$, where $\nu_T(\mathbf{x})$ is the eddy viscosity, $\bar{S}_{ij} = \frac{1}{2}(\partial \bar{u}_i/\partial x_j + \partial \bar{u}_j/\partial x_i)$ is the resolved strain rate, and δ_{ij} is the Kronecker delta function. The dynamic Smagorinsky model [3] is particularly popular. The dynamic Smagorinsky model is purely dissipative, and therefore stabilizing. Its success is due to its ability to control dissipation according to the local flow state. This dynamic mechanism is achieved by use of the Germano identity and a scale-invariance assumption, and does not require any adjustable constants. A wide range of flows have therefore been successfully computed using this modeling approach.

However, from a theoretical standpoint, eddy viscosity models have some limitations. They cannot predict backward dissipation [4], *a priori* tests show that their correlation with the true SGS stress is very low [5], and their underlying local equilibrium hypothesis is questionable [6]. These limitations do not appear to cause serious problems in practical LES, because the dynamic Smagorinsky model performs quite well at moderate resolutions. However, this is not the case for highly under-resolved LES; e.g. channel flow where the near-wall region is not resolved. Alternative SGS models are perhaps required at coarse resolutions where the underlying assumptions of eddy viscosity, small-scale isotropy and universality of SGS motion, are no longer valid.

An alternative approach to eddy-viscosity models is sometimes termed 'structural modeling' [7]. Here, interactions with the subgrid scales are modeled in terms of interactions between larger and smaller resolved scales. Scale similarity models [8,9] fall into this category; e.g. Liu et al.'s model [9], $\tau_{ij} = C_L(\widetilde{\bar{u}_i \bar{u}_j} - \widetilde{\bar{u}}_i \widetilde{\bar{u}}_i)$, where the tilde denotes filtering at $\widetilde{\Delta}$ larger scales than Δ, and $C_L = \mathrm{O}(1)$ is the closure coefficient. Such models show very high correlation with the true SGS stress in *a priori* tests with smooth invertible filters, but become completely uncorrelated with the true SGS stress when sharp cut-off filters are used [9,10]. More importantly, most similarity models suffer from the lack of adequate SGS dissipation in actual LES [5,10]. The resulting instability is often attributed to excessive backscatter by the similarity model. This explanation is however incomplete since the true SGS stress also has large levels of backward dissipation. A less discussed limitation of the similarity model concerns its spectral behavior. Liu et al.'s model [9] for example, vanishes at scales smaller than $\widetilde{\Delta}$, as is evident from its formulation. On the other hand, DNS data [11–13] shows that the most significant contribution of SGS force to the resolved solution lies in the narrow band very to near the cut-off wavenumber. These limitations result in very poor performance in *a posteriori* tests; e.g. LES of forced isotropic turbulence [10]. Although mixed models [14,15,5,13] can improve the stability by adding an eddy viscosity term, the problems associated with the similarity term remain unaddressed. For example, see [10] for results and discussion of the dynamic two-component model [13].

We therefore consider an alternative modeling approach; models based on the estimation of SGS velocity [16–21]. SGS models using u'_i have backward dissipation, allow SGS kinetic energy to be computed, and are free from the local equilibrium hypothesis and linear stress–strain relationship. Also, modeling the subgrid

scale velocity is attractive for flows involving scalar mixing, chemical reaction, particles, and liquid sprays that have important physical effects occurring at subgrid scales. In such situations, once the subgrid velocity is obtained, the subgrid phenomena can be modeled more easily using their unfiltered governing equations.

However, a fundamental issue for such models is that the SGS velocity u_i', by definition, cannot be represented on the LES grid. Two distinct approaches have been proposed in the literature to overcome this problem. The first approach is to use a fully resolved, but reduced dimensional (typically one-dimensional) model to obtain the unresolved velocity, e.g. [16,17]. Another approach is to use a three-dimensional finer (but still under-resolved) grid to obtain u_i', e.g. [18,19]. There also exist SGS estimation models based on one-dimensional fractal interpolation [21] and subgrid vorticity estimation [20].

The objective of this paper is to propose a simple approach that combines the dissipative nature of eddy viscosity models with more physically appealing, structural SGS models. This is accomplished in two steps. First, a new subgrid scale model (RSEM) is proposed, which estimates the unresolved velocity field in physical space. The SGS velocity components are evaluated on the LES grid, without requiring finer grids. The model has an unknown coefficient, which is determined such that the resulting SGS dissipation is constrained by that obtained from an eddy viscosity model. The proposed model can be easily implemented into existing LES solvers that use eddy viscosity models. The performance of the proposed model is evaluated using various *a priori* and *a posteriori* tests on decaying isotropic turbulence and turbulent channel flow (Sections 3 and 4). Two variants of the model, and different approaches to imposing SGS dissipation as a constraint are evaluated. Both statistics and instantaneous flow structures are compared to those from the target eddy viscosity model, in order to study how the proposed model is different from the target eddy viscosity model. The main strengths and weaknesses of the proposed model are discussed in Section 5.

2. Proposed model

2.1. Formulation

The first step is to approximate the SGS velocity on the LES grid. At first glance, approximating the SGS velocity u_i' on the LES grid does not make sense. However, this approach can be justified by noting that our ultimate goal is to obtain the SGS stress

$$\tau_{ij} = \overline{\bar{u}_i u_j'} + \overline{u_i' \bar{u}_j} + \overline{u_i' u_j'}. \tag{3}$$

Here, τ_{ij} is a grid scale quantity, which means that τ_{ij} and $\bar{u}_i$ have the same spectral support and τ_{ij} can therefore be expressed as a function of $\bar{u}_i$. There exists a 'resolved projection' of SGS velocity, u_i^{rsg} such that the modeled SGS stress

$$\tau_{ij}^M = \bar{u}_i u_j^{\mathrm{rsg}} + u_i^{\mathrm{rsg}} \bar{u}_j + u_i^{\mathrm{rsg}} u_j^{\mathrm{rsg}} \tag{4}$$

approximates the true SGS stress τ_{ij} within a suitably defined error measure. Note that Eq. (4) does not have the global over-bar unlike true SGS stress (3), since $\bar{u}_i$, u_i^{rsg} and τ_{ij}^M are defined on the same LES grid. The model performance depends on the model for resolved projection u_i^{rsg}. From dimensional considerations, u_i^{rsg} is modeled as

$$u_i^{\mathrm{rsg}} = R\theta \mathcal{N}_i, \tag{5}$$

where R is an adjustable constant, θ is a time scale and $\mathcal{N}_i$ is a nonlinear term. We set $\theta = \Delta / U_{\mathrm{ref}}$, where U_{ref} is a reference velocity. For example, U_{ref} is equal to the initial rms velocity fluctuation u_{rms}, and the bulk velocity U_{b} for isotropic turbulence and channel flow respectively. θ makes R dimensionless; the dynamic behavior of the model is mostly determined by the nonlinear term

$$\mathcal{N}_i = \bar{u}_j \mathcal{L}_{ij}, \tag{6}$$

where $\mathcal{L}_{ij}$ is a linear tensor with the same dimensions as velocity gradient. Two candidates, $\mathcal{L}_{ij}^{(1)} = \partial \bar{u}_i / \partial x_j = \overline{D}_{ij}$ and $\mathcal{L}_{ij}^{(2)} = \overline{S}_{ij}$ are considered in this paper. Here, D_{ij} and S_{ij} are the deformation and strain-rate tensors respectively. These choices of $\mathcal{L}_{ij}$ are based on dimensional and spectral considerations. Although the spectral behavior of the resolved projection u_i^{rsg} is unknown, the synthetic SGS stress τ_{ij}^M should scale with $\mathcal{N}^2$. The velocity

gradient emphasizes the smallest resolved scales, as required by the spectral behavior of the exact SGS stress. $\mathcal{L}_{ij}^{(1)}$ is suggested by the nonlinear term in the Navier–Stokes equations and the work of [18]. However, the choice of $\mathcal{L}_{ij}^{(2)} = \overline{S}_{ij}$ is essentially *ad hoc*, and is adopted after numerical experiments in which the model with $\overline{S}_{ij}$ outperforms that with $\overline{D}_{ij}$. Once u_i^{rsg} is obtained, the synthetic SGS stress is readily given by (4). The proposed model will be referred to as *resolved-subgrid scale estimation model* (RSEM). Also, the model corresponding to the two forms of $\mathcal{L}_{ij}$ will be referred to as RSEM-S and RSEM-D, respectively.

The above form of the model violates Galilean invariance [22], which requires that the system (1) be form-invariant under the observer transformation $\mathbf{x}^* = \mathbf{x} + \mathbf{V}t + \mathbf{b}$, where $\mathbf{V}$ and $\mathbf{b}$ are constant vectors. Applying this transformation to the true SGS stress yields

$$\tau_{ij}^* = \tau_{ij} + V_i\overline{u_j'} + V_j\overline{u_i'}, \tag{7}$$

where the Galilean invariance of SGS velocity $\mathbf{u}'^* = \mathbf{u}'$ is invoked. It is easy to see that the invariance error is zero when $\overline{u_i'} = 0$, which is the case for the cut-off filter. For RSEM, however, $\mathbf{u}^{\mathrm{rsg}*} \neq \mathbf{u}^{\mathrm{rsg}}$ since u_i^{rsg} is a resolved scale quantity unlike true SGS velocity. Furthermore, it is impossible to satisfy Galilean invariance by modifying u_i^{rsg} such that $\mathbf{u}^{\mathrm{rsg}*} = \mathbf{u}^{\mathrm{rsg}}$, because in that case modeled SGS stress would be $\tau_{ij}^{M*} = \tau_{ij}^M + V_i u_j^{\mathrm{rsg}} + V_j u_i^{\mathrm{rsg}}$, and the invariance is satisfied only when $u_i^{\mathrm{rsg}} = \tau_{ij}^M = 0$. We adopt a simple remedy to enforce Galilean invariance by modifying the model to not have any mean contribution; i.e.

$$\tau_{ij}^M(\bar{\mathbf{u}}) \rightarrow \tau_{ij}^M(\bar{\mathbf{u}} - \mathbf{U}_{\mathrm{b}}), \tag{8}$$

where $U_{\mathrm{b},i}$ is the bulk velocity of the entire flow. All expressions involving the resolved velocity $\bar{u}_i$ in (5) and (6) are replaced by $\bar{u}_i - U_{\mathrm{b},i}$. It is readily seen that the SGS stress $\tau_{ij}^M(\bar{\mathbf{u}} - \mathbf{U}_{\mathrm{b}})$ is invariant under Galilean transformation. Note that the bulk velocity can change without changes in the local state, for example, by expanding the domain along inhomogeneous directions. As a result of using the bulk velocity to enforce Galilean invariance, changing the bulk velocity might change the local modeled stress. All results shown in the following sections are obtained using this Galilean invariant formulation.

2.2. Coefficient determination

The coefficient R in Eq. (5) is determined from a constraint on the SGS dissipation; i.e. the modeled SGS dissipation is forced to approximate a target value of the SGS dissipation. In principle, the target dissipation could be obtained from any model; here it is obtained from the dynamic Smagorinsky model [3]:

$$\tau_{ij}^t - \frac{1}{3}\tau_{kk}^t\delta_{ij} = -2(C_s\Delta)^2|\overline{S}|\overline{S}_{ij}, \tag{9}$$

where $|\overline{S}| = \sqrt{2\overline{S}_{ij}\overline{S}_{ij}}$, $(C_s\Delta)^2 = \langle L_{ij}M_{ij}\rangle_{h,+}/\langle M_{ij}M_{ij}\rangle_h$, $L_{ij} = \widetilde{\overline{u}_i\overline{u}_j} - \widetilde{\overline{u}}_i\widetilde{\overline{u}}_j$, and $M_{ij} = (\widetilde{\Delta}/\Delta)^2|\widetilde{\overline{S}}|\widetilde{\overline{S}}_{ij} - |\overline{S}|\widetilde{\overline{S}}_{ij}$. Here, the tilde denotes test filtering at $\widetilde{\Delta} = 2\Delta$, $\langle\cdots\rangle_h$ is an average over homogeneous direction(s), and $\langle\phi\rangle_+ = 0.5(\langle\phi\rangle + |\langle\phi\rangle|)$ is clipping for positive eddy viscosity. The superscript t represents the target value. From τ_{ij}^t, we determine the 'target SGS dissipation' $D^t = \tau_{ij}^t\overline{S}_{ij} = (\tau_{ij}^t - \frac{1}{3}\tau_{kk}^t\delta_{ij})\overline{S}_{ij}$.

The coefficient R is chosen such that it minimizes the difference between the dissipation obtained from RSEM and the target dissipation. This can be done in a number of ways. We define $\tau_{ij}^M = \bar{u}_i u_j^{\mathrm{rsg}} + u_i^{\mathrm{rsg}}\bar{u}_j + u_i^{\mathrm{rsg}}u_j^{\mathrm{rsg}}$ as the SGS stress predicted by RSEM. We exclude the trivial condition

$$\tau_{ij}^M\overline{S}_{ij} = D^t \tag{10}$$

because τ_{ij}^M would then have the same drawbacks as the purely dissipative target model. It is desirable that SGS dissipation be equal to D^t only in the mean, and have large forward and backward dissipation, similar to the true SGS dissipation. τ_{ij}^M is therefore constrained by the ensemble average of D^t; i.e.

$$\langle\tau_{ij}^M\overline{S}_{ij}\rangle = \langle D^t\rangle, \tag{11}$$

where $\langle\ \rangle$ denotes the ensemble average. Note that Eq. (11) can be local in space for complex flows; also R is constant with respect to the ensemble. Inserting (5) into (11), we obtain

$$\langle(\bar{u}_i u_j^{\mathrm{rsg}} + u_i^{\mathrm{rsg}}\bar{u}_j + u_i^{\mathrm{rsg}}u_j^{\mathrm{rsg}})\overline{S}_{ij}\rangle = \langle R\theta(\bar{u}_i\mathcal{N}_j + \bar{u}_j\mathcal{N}_i)\overline{S}_{ij} + R^2\theta^2\mathcal{N}_i\mathcal{N}_j\overline{S}_{ij}\rangle = \langle D^t\rangle. \tag{12}$$

Since R is assumed to be constant with respect to the ensemble average, (12) reduces to

$$\langle\alpha\rangle R^2 + \langle\beta\rangle R = \langle D^t\rangle, \tag{13}$$

where $\alpha = \theta^2 \mathcal{N}_i \mathcal{N}_j \overline{S}_{ij}$ and $\beta = \theta(\bar{u}_i \mathcal{N}_j + \bar{u}_j \mathcal{N}_i)\overline{S}_{ij}$. When the ensemble average is performed with respect to time, it is not possible to obtain R from (13) unless $\langle\alpha\rangle$, $\langle\beta\rangle$, and $\langle D^t\rangle$ are known *a priori*. The ensemble average is therefore approximated by a cumulative average until steady values of $R(\mathbf{x})$ are obtained. The use of a cumulative average may give the impression that the model could be erroneous during initial transients. However, even at very short times, R is properly determined from the instantaneous or short-time averaged SGS dissipation predicted by the dynamic Smagorinsky model. For homogeneous flows, it is reasonable to compute the ensemble average by averaging over the entire volume so that R is a function of time, and constant in space. This is the case for decaying isotropic turbulence, which will be discussed in the next section. The two possible solutions to the quadratic Eq. (13) are readily computed; of these the solution that minimizes the following least-square error $\mathcal{F}(R)$ is chosen:

$$\mathcal{F}(R) = \int_\Omega (\tau_{ij}^M \overline{S}_{ij} - D^t)^2 \mathrm{d}\mathbf{x} = \int_\Omega (\alpha R^2 + \beta R - D^t)^2 \mathrm{d}\mathbf{x}. \tag{14}$$

However, the fact that Eq. (13) does not guarantee real roots means that 'matching total SGS dissipation' is not always possible. In this case, R should be given by an alternative condition which guarantees a real solution. R that minimizes the least-square error $\mathcal{F}(R)$ seems to be a rational choice. Such R is given by the solution to $\partial\mathcal{F}/\partial R = 0$, yielding

$$R^3 \int_\Omega 2\alpha^2 \,\mathrm{d}\mathbf{x} + R^2 \int_\Omega 3\alpha\beta \,\mathrm{d}\mathbf{x} + R \int_\Omega (\beta^2 - 2\alpha D^t)\mathrm{d}\mathbf{x} - \int_\Omega \beta D^t \,\mathrm{d}\mathbf{x} = 0. \tag{15}$$

Since Eq. (15) is a cubic equation, the existence of real solution is guaranteed. In the case of multiple roots, the root that yields the smallest values of

$$\left| \int_\Omega \tau_{ij}^M \overline{S}_{ij} \,\mathrm{d}\mathbf{x} - \int_\Omega D^t \,\mathrm{d}\mathbf{x} \right| \tag{16}$$

can be chosen. However, it is observed that (15) has only one real root R for all the numerical examples considered in this paper. This method will be referred to as 'least-square method'. Since $\mathcal{F}(R)$ has the form of a L_2-error, $\tau_{ij}^M \overline{S}_{ij}$ may be viewed as 'the best approximation' to D^t [23] by a lower dimensional approximation to D^t when R is assumed constant. However, if arbitrary variation of R is allowed, the minimization of (14) is meaningless since it will then reduce to (10). All results in the subsequent sections are based on the 'matching global dissipation' unless otherwise specified. Numerical experiments with 'least-square method' are performed for both RSEM-S and RSEM-D for channel flow in Section 4.2.

In summary, the procedure to obtain R is as follows. Solve the quadratic Eq. (13). If both roots are real, compute the functional (14) and choose the root which yields the smaller value. If (13) does not have real roots, solve the cubic Eq. (15). If all roots of (15) are real, compute the functional (16) and choose the root which yields the smallest value. If (15) has one real root and a complex conjugate pair, choose the real root.

For channel flow, $R = R(y)$ is a function of the wall-normal coordinate, and the same procedure as homogeneous flow, is applied over each homogeneous plane. Once R is computed, it is inserted into (5) and (4) to construct τ_{ij}^M. A practical advantage of the proposed model is that it can be easily implemented in existing LES codes with eddy viscosity models. Once the target dissipation is obtained, RSEM is constructed at negligible additional cost. The only additional step is to compute R by using either (13) or (15). Virtually no additional CPU time was required for this step in the isotropic turbulence and channel flow problems considered in this study.

3. Results: isotropic turbulence

3.1. A priori tests

Appropriate spectral behavior is essential if SGS models are to properly represent interscale energy transfer. However, the constraint on total SGS dissipation offers no guarantees on the spectral behavior of

the proposed model. An *a priori* test is therefore performed on RSEM to compare the spectral behavior of predicted SGS stress to that from the dynamic Smagorinsky model, and the true SGS stress.

Consider a synthetic field of isotropic turbulence with random Fourier phases for the velocity field and Fourier magnitudes chosen to satisfy the von Kármán spectrum

$$E(k) = \frac{2.683k^4}{(0.417 + k^2)^{17/6}}. \tag{17}$$

The spectrum is normalized such that $E(k) = 1$ at $k = 1$. Fig. 1 shows the power spectrum of SGS force obtained from the dynamic Smagorinsky model, RSEM and analytical bounds [1] at the cut-off wavenumber $k_c = 8$

$$\mathcal{S}(k) = 4\pi k^2 \lim_{L\to\infty} \left(\frac{2\pi}{L}\right)^3 \langle F_i(\mathbf{k}) F_i^*(\mathbf{k})\rangle_k.$$

Here, $F_i(\mathbf{k}) = ik_n P_{im}(\mathbf{k})\hat{\tau}_{mn}(\mathbf{k})$ is the SGS force combined with pressure term, $P_{im}(\mathbf{k}) = \delta_{im} - k_i k_m/k_l k_l$ is the projection tensor, L is the domain size and $\langle\phi\rangle_k$ is the spherical shell average at $k = |\mathbf{k}|$. The SGS force for the dynamic Smagorinsky model and RSEM are computed numerically as described in Ref. [24]. Fig. 1 shows that the power spectrum from RSEM-S is within theoretical bounds, and is similar to that from the dynamic Smagorinsky model. RSEM-S therefore has appropriate spectral behavior in the sense that the SGS force is maximum at the cut-off wavenumber and negligible at small wavenumbers [13,11,12]. This behavior is due to the nonlinear term $\mathcal{N}_i = \bar{u}_j \mathcal{L}_{ij}$ being parametrized in terms of velocity derivatives, which are weighted towards higher wavenumber regions. Note that the power spectrum of RSEM-D deviates more from the dynamic Smagorinsky model, suggesting that the SGS stress for this model can be quite different, in spite of the constraint on SGS dissipation. Results from RSEM-D may therefore show large variation from the dynamic Smagorinsky model.

3.2. A posteriori tests

The proposed model is applied to the decaying isotropic turbulence experiments of Comte-Bellot and Corrsin [25]. The Taylor micro-scale Reynolds number $Re_\lambda = u_{\rm rms}\lambda/\nu$ decays from 71.6 to 60.6 in the experiments. LES is performed using a dealiased spectral method at 32^3 and 64^3 resolutions, and semi-implicit time integration (see [26] for numerical details). Since the proposed models are neither purely eddy viscosity models nor unconstrained estimation models, their performance is compared to both the dynamic Smagorinsky model and a subgrid scale estimation model by Domaradzki and Loh [18].

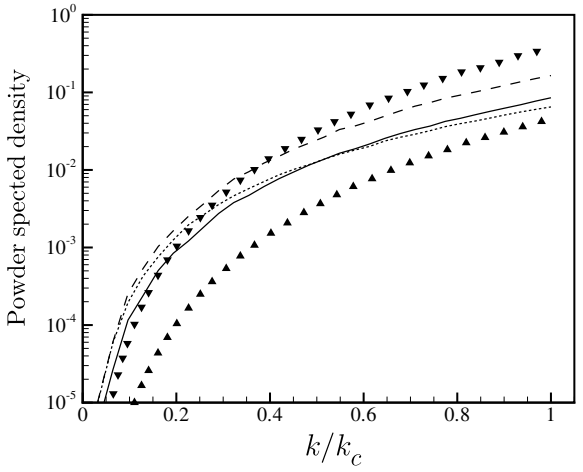

Fig. 1. Power spectral densities of SGS force for isotropic turbulence with von Karman spectrum. ▲ and ▼, lower and upper bounds of theoretical SGS force [1]; ···, dynamic Smagorinsky model; —, RSEM-S; ---, RSEM-D.

Fig. 2 shows three-dimensional energy spectra at non-dimensional time $tU_0/M = 42$, 98 and 171. Also shown is the time evolution of resolved kinetic energy. $M = 5.08$ cm and $U_0 = 10$ m/s denote the experimental grid size and the mean convection velocity, respectively. Note that the resolved kinetic energy is normalized by its initial value at $tU_0/M = 42$ at both resolutions. All values except time in the figures of this section are non-dimensionalized by reference velocity $u_{\text{ref}} = \sqrt{\frac{3}{2}}u_{\text{rms}}$ and length scale $L_{\text{ref}} = 11M$. It appears that the estimation model proposed by Domaradzki and Loh [18] lacks dissipation, and yields noticeable pile-up of energy at high-wavenumbers. This behavior is consistent with previous results for forced isotropic turbulence obtained with this model [19,10]. Results from the dynamic Smagorinsky model and RSEM show good agreement with the experimental data. Note that the spectra from RSEM-S are very close to that from the dynamic Smagorinsky model. On the other hand, RSEM-D predicts faster decay of the resolved kinetic energy, and underpredicts the energy spectra. These results demonstrate that (i) estimating the SGS velocity from resolved projection yields similar spectral distribution of SGS stress to dynamic Smagorinsky model, (ii) the dissipation constraint method works successfully, and (iii) RSEM-S yields better predictions than RSEM-D. Also note that the qualitative behavior of the model are insensitive to grid resolution. Therefore, only results from 32^3 resolution will be shown in the following discussion.

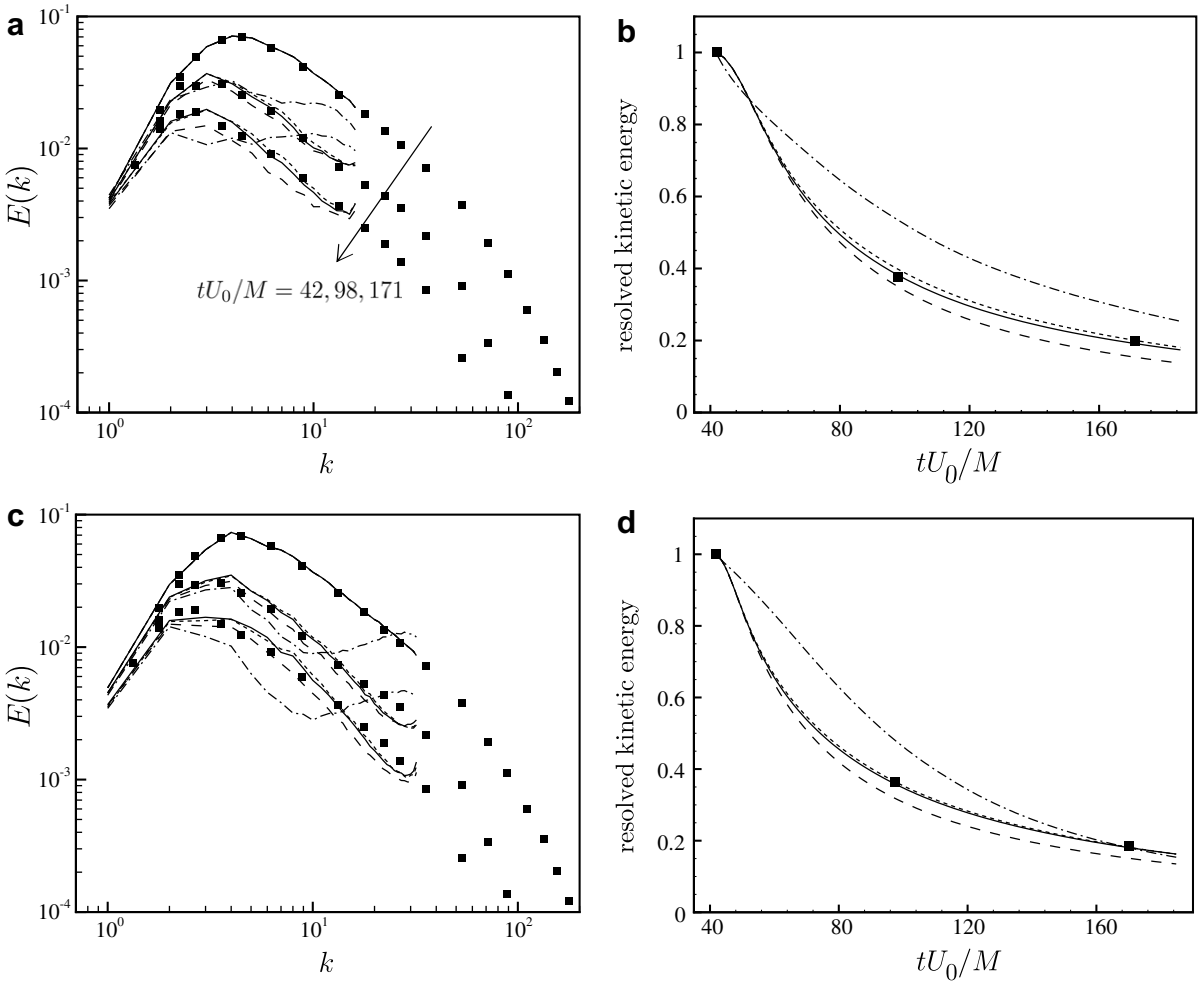

Fig. 2. Decaying isotropic turbulence from LES with various SGS models: (a) and (c) three-dimensional energy spectra at $tU_0/M = 42, 98$ and 171; (b) and (d) time evolution of resolved kinetic energy. ■, Comte-Bellot and Corrsin [25]; -·-·-, subgrid scale estimation model [18]; · · ·, dynamic Smagorinsky model; - - -, RSEM-D; —, RSEM-S. (a) and (b) are from LES results at 32^3 resolution and (c) and (d) are from results at 64^3 resolution.

3.3. Differences between RSEM and dynamic Smagorinsky model

It may be argued that the above results are to be expected since LES of isotropic turbulence is dominated by SGS dissipation, which is in some sense, 'prescribed'. We therefore examine the deviation of both forms of RSEM from the dynamic Smagorinsky model. First, the correlation between subgrid stresses is computed; i.e.,

$$\rho(\tau_{ij}^{\mathrm{DSM}}, \tau_{ij}^{\mathrm{RSEM}}) = \frac{\langle \tau_{ij}^{\mathrm{DSM}} \tau_{ij}^{\mathrm{RSEM}} \rangle}{\langle \tau_{ij}^{\mathrm{DSM}} \tau_{ij}^{\mathrm{DSM}} \rangle^{1/2} \langle \tau_{ij}^{\mathrm{RSEM}} \tau_{ij}^{\mathrm{RSEM}} \rangle^{1/2}}. \tag{18}$$

This tensor-level correlations reach steady values $\rho(\tau_{ij}^{\mathrm{DSM}}, \tau_{ij}^{\mathrm{RSEM}-\mathcal{S}}) \approx 0.57$, and $\rho(\tau_{ij}^{\mathrm{DSM}}, \tau_{ij}^{\mathrm{RSEM}-\mathcal{D}}) \approx 0.34$. Whereas, scalar-level correlation, or the correlation between the SGS dissipation $\epsilon = \tau_{ij}\overline{S}_{ij}$ is similarly computed and obtained as $\rho(\epsilon^{\mathrm{DSM}}, \epsilon^{\mathrm{RSEM}-\mathcal{S}}) \approx 0.83$, and $\rho(\epsilon^{\mathrm{DSM}}, \epsilon^{\mathrm{RSEM}-\mathcal{D}}) \approx 0.65$. As expected from Figs. 1 and 2, the RSEM-S model predictions of the SGS dissipation and subgrid stress are better correlated with the dynamic Smagorinsky model. Also note that for both formulations, the correlations in SGS dissipation are higher than that for the subgrid stress. This behavior is consistent with the SGS dissipation being imposed as a global constraint. The relatively low correlations in the SGS stress suggests that the model structure of the RSEM is fundamentally different from the dynamic Smagorinsky model. This conjecture is assessed in Fig. 3 by plotting the joint p.d.f. between both models. Fig. 3 shows joint p.d.f.s of SGS stress and SGS dissipation at $tU_0/M = 120$. The lower SGS dissipation correlation of the RSEM-D is due to its relatively large levels of backward dissipation (Fig. 3(b)). On the other hand, RSEM-S shows small levels of backscatter and is therefore more correlated with the purely dissipative dynamic Smagorinsky model. Fig. 3(a) shows that the stresses predicted by the RSEM-D and dynamic Smagorinsky models are nearly uncorrelated. The shape of the SGS stress p.d.f. suggests that RSEM-D yields higher rms values of SGS stress than either RSEM-S or the dynamic Smagorinsky model. This behavior is consistent with the power spectrum of SGS force shown in Fig. 1. Thus, we can conclude that (i) RSEM-S works at least as well as the dynamic Smagorinsky model, (ii) the SGS stresses predicted by RSEM are quite different from the dynamic Smagorinsky model, and (iii) the formulation based on the strain-rate results in the dominance of forward dissipation, and is therefore more correlated with the dynamic Smagorinsky model.

3.4. Interaction between dynamic Smagorinsky model and RSEM

The dynamic constant and target SGS dissipation obtained from the dynamic Smagorinsky model in the RSEM code, will be different from those obtained from a LES code that only uses the dynamic Smagorinsky

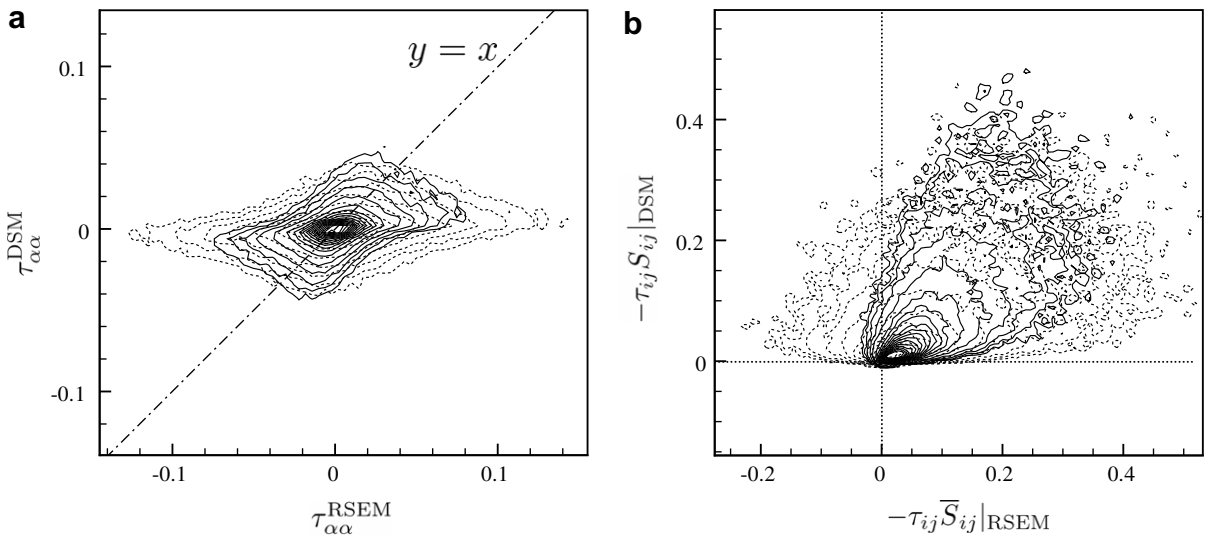

Fig. 3. Joint PDF between dynamic Smagorinsky model and RSEM at $tU_0/M = 128$ for decaying isotropic turbulence at 32^3 resolution: (a) normal component of SGS stress; (b) SGS dissipation. ···, RSEM-D; —, RSEM-S.

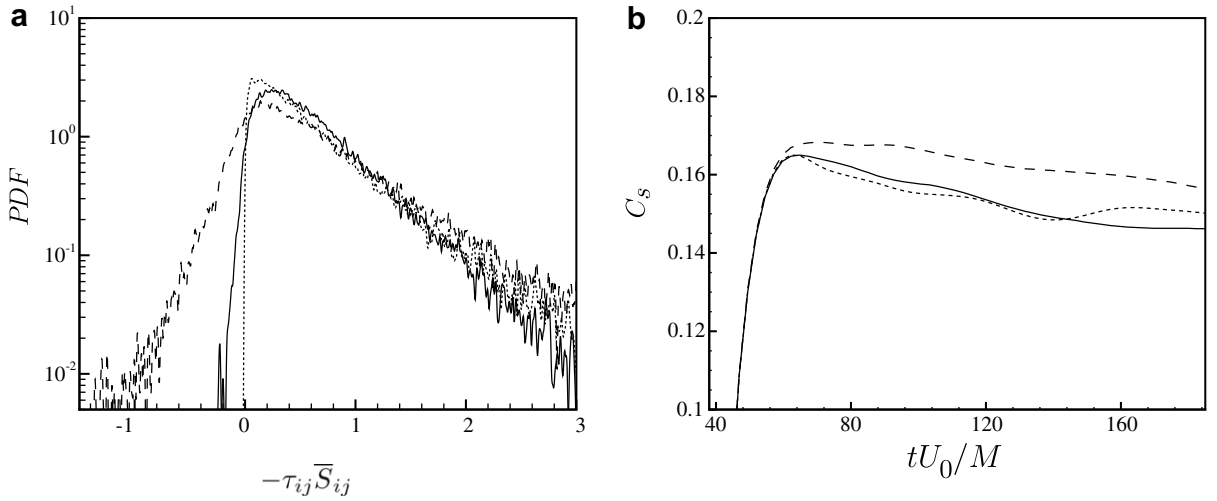

Fig. 4. Interaction between dynamic Smagorinsky model and RSEM: (a) p.d.f. of SGS dissipation at $tU_0/M = 60$ and (b) time evolution of the Smagorinsky constant C_s for decaying isotropic turbulence at 32^3 resolution. ···, Dynamic Smagorinsky model; ---, RSEM-D; —, RSEM-S.

model. This dynamic interaction is examined in terms of the SGS dissipation. Fig. 4 shows the p.d.f. of SGS dissipation at $tU_0/M = 60$, along with time evolution of the dynamic Smagorinsky constant, C_s. It is interesting that RSEM-D shows more dissipative behavior in the energy spectra and total kinetic energy, in spite of showing higher levels of backscatter (Fig. 2). This behavior is a result of the interaction among the resolved field, dynamic Smagorinsky model predictor, and RSEM. It is seen that C_s increases significantly for RSEM-D. Thus, it appears that RSEM-D predicts large backscatter across the cut-off, which increases energy at the smallest resolved scale, which in turn increases C_s. Increased values of C_s increase the target SGS dissipation, D^t. A stable solution is thus obtained inspite of high backscatter. Although RSEM-D is less accurate than RSEM-S, the compatibility of large backscatter with solution stability is an encouraging feature of the RSEM approach.

4. Results: turbulent channel flow

LES of turbulent channel flow at $Re_\tau = u_\tau\delta/\nu = 180$ and 590 is performed using a dealiased pseudo-spectral code [27] similar to Kim et al. [28], where the governing equations are written in term of the Laplacian of wall-normal velocity ($\nabla^2 v$) and vorticity ($\mathrm{d}u/\mathrm{d}z - \mathrm{d}w/\mathrm{d}x$). Here, δ denotes the channel half height and u_τ denotes the friction velocity. Fourier expansion is used in the streamwise (x) and spanwise (z) directions, and the Chebyshev-tau method is used in the wall-normal (y) direction. The nonlinear term is written in rotational form, and is computed using pseudo-spectral method with 3/2-rule dealiasing in x, z directions. Third-order Runge–Kutta and Crank–Nicolson schemes are used for time integration of the nonlinear terms and viscous terms, respectively. Subgrid terms are treated explicitly as part of nonlinear term. For the test filtering of the dynamic Smagorinsky model, the Fourier cut-off filter is applied parallel to the wall with filter width ratio of 2 in each direction. No test filter is applied in the wall-normal direction. A constant body force is added to the right-hand

Table 1
Computational parameters for LES of turbulent channel flow

Run	Re_τ	Domain ($x \times y \times z$)	Grid ($x \times y \times z$)	Resolution
Case I	180	$2\pi\delta \times 2\delta \times \pi\delta$	$16 \times 48 \times 16$	$\Delta x^+ = 70,\ \Delta z^+ = 35$
Case II	590	$\pi\delta \times 2\delta \times 0.5\pi\delta$	$24 \times 96 \times 32$	$\Delta x^+ = 77,\ \Delta z^+ = 29$
Case III	590	$\pi\delta \times 2\delta \times 0.5\pi\delta$	$12 \times 96 \times 16$	$\Delta x^+ = 154,\ \Delta z^+ = 58$

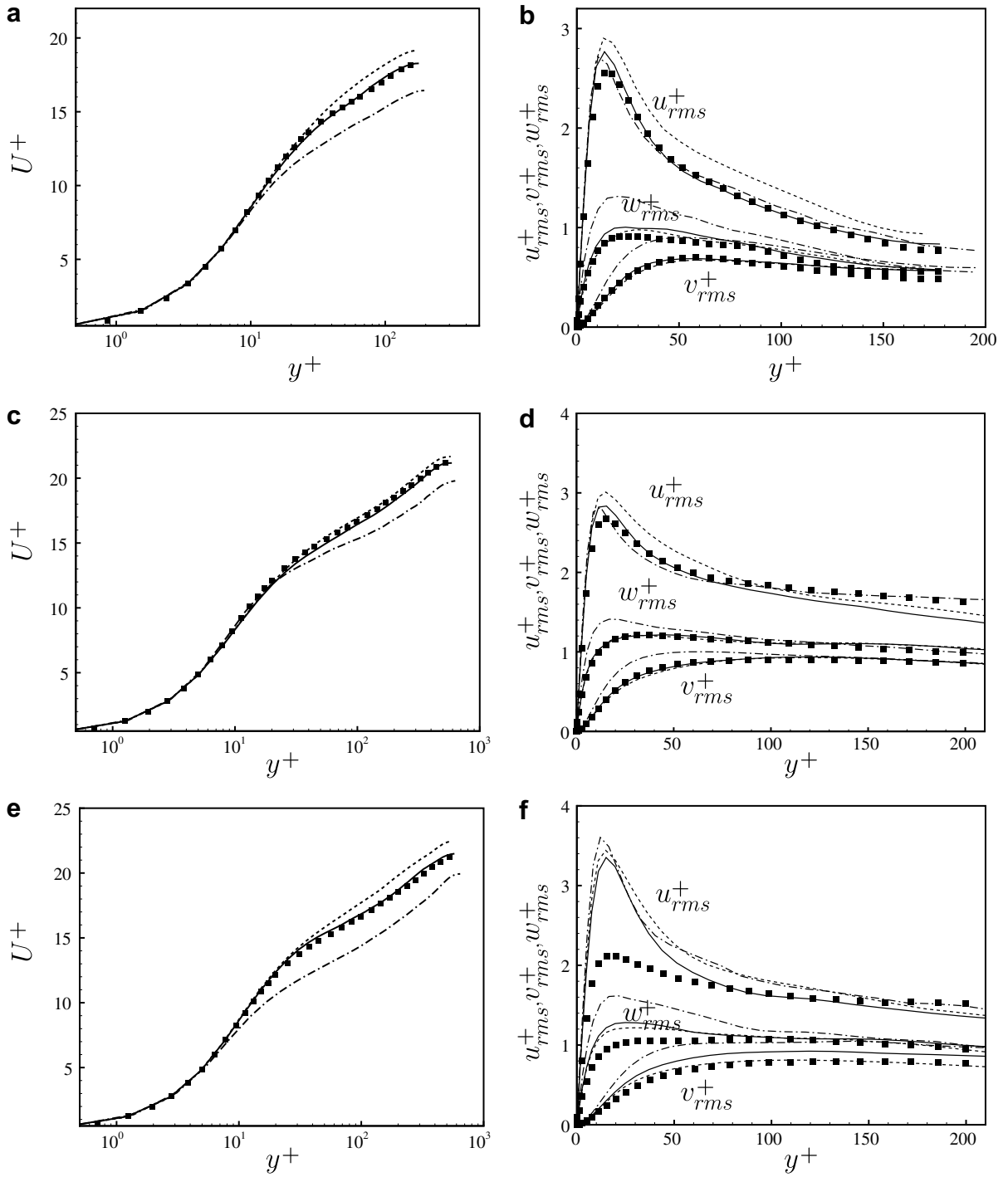

Fig. 5. Flow statistics of turbulent channel flow at $Re_\tau = 180$ and $Re_\tau = 590$ from filtered DNS (■), LES with dynamic Smagorinsky model (···), RSEM-S (—), and LES without SGS model (-·-·-): (a), (c) and (e) mean streamwise velocities; (b), (d) and (f) RMS velocity fluctuations; (a) and (b) Case I; (c) and (d) Case II; (e) and (f) Case III.

side of the u-momentum equation to drive the flow at fixed mass flow rate. Thus, wall-shear stress and u_τ are not fixed and even their mean values can be different in each LES due to modeling errors. Since all results shown in this section are based on wall units from each case, the results also reflect the differences in the wall shear stress.

The domain size, grid and resolution used in the simulations are summarized in Table 1. Note that Cases I and II marginally resolve near-wall structures, while Case III corresponds to a wall-unresolved simulation. Note that the wall-normal resolution is quite good; i.e., we assume that the grid filter is applied only to the wall-parallel directions. Case III is considered wall-unresolved due to its coarse streamwise and spanwise resolutions. Along with LES, DNS were performed at the same Reynolds numbers and with the same domain sizes to obtain 'filtered' DNS data (denoted as fDNS). The filtered data were obtained at LES resolutions using the Fourier cut-off filter in wall-parallel (x and z) directions. Note that the present DNS and LES use half the domain sizes as Kim et al. [28] and Moser et al. [29]. Ref. [27] shows that all the statistics considered in this paper are virtually unaffected by the reduced domain size.

Fig. 5 shows mean velocity and RMS velocity fluctuations from the filtered DNS, LES using the dynamic Smagorinsky model, RSEM-S, and no SGS model. Only RSEM-S results are shown here for clarity. Results from the RSEM-D model are presented at the end of this section. Note that in the absence of the SGS model, the normalized velocities are highly under-estimated, showing the importance of the SGS models to the computed solutions.

The performance of the dynamic Smagorinsky model is good, but still lacking in that it overpredicts the streamwise velocity fluctuations and mean velocity in the log region. This is especially true for the low Reynolds number case, $Re_\tau = 180$ shown in Fig. 5(a). This trend has long been known, since essentially the same results were observed by Germano et al. [3], who attributed the overprediction of mean velocity to the underestimation of wall skin friction by insufficient resolution. From Fig. 5, it appears that the RSEM model corrects this behavior. LES with the RSEM model yields more accurate mean velocity profiles and RMS fluctuations for all cases, especially for the well-resolved Cases I and II. For Case III where the near-wall structures are highly unresolved, both models overpredict u_{rms}. However, even for this case, RSEM yields better predictions for the mean velocity. Computed values of Re_τ and error in the skin friction (C_f) from all models are summarized in Table 2. Note that the RSEM model shows less than 4% error in the skin friction.

Table 2
Computed Re_τ and errors in skin friction

	Case I		Case II		Case III	
	Re_τ	ΔC_f (%)	Re_τ	ΔC_f (%)	Re_τ	ΔC_f (%)
fDNS	178	...	587	...	587	...
No model	195	20.0	631	15.6	644	20.4
DSM	172	−6.6	578	−3.0	554	−10.9
RSEM	178	−0.2	591	1.4	576	−3.7

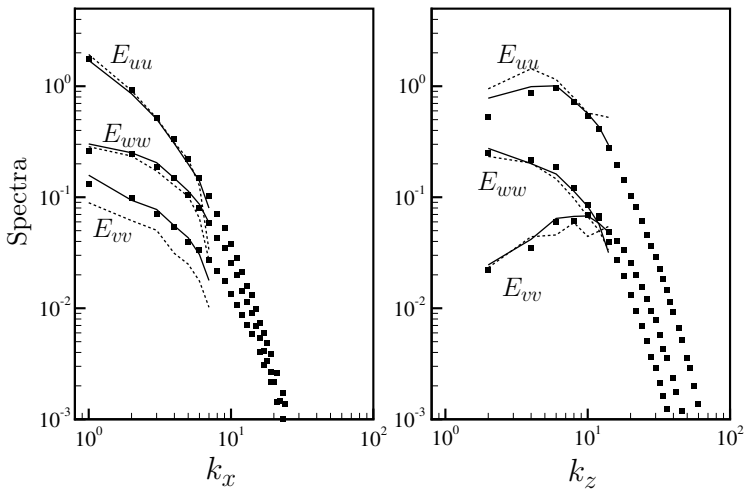

Fig. 6. The effect of SGS model on the (a) streamwise and (b) spanwise velocity spectra at $y^+ = 30$ of turbulent channel flow at $Re_\tau = 180$ (Case I). ■, DNS; ···, dynamic Smagorinsky model; —, RSEM-S.

4.1. Difference between RSEM and the dynamic Smagorinsky model

The improved prediction of the RSEM model is associated with changes in flow structure. Velocity spectra at $y^+ = 30$ and instantaneous vortical structures visualized by the positive Q-criteria [30] are computed for Case I and shown in Figs. 6 and 7, respectively. Note that the spectra and vortical structures predicted by RSEM show better agreement with filtered DNS than the dynamic Smagorinsky model. The 'ejection' or

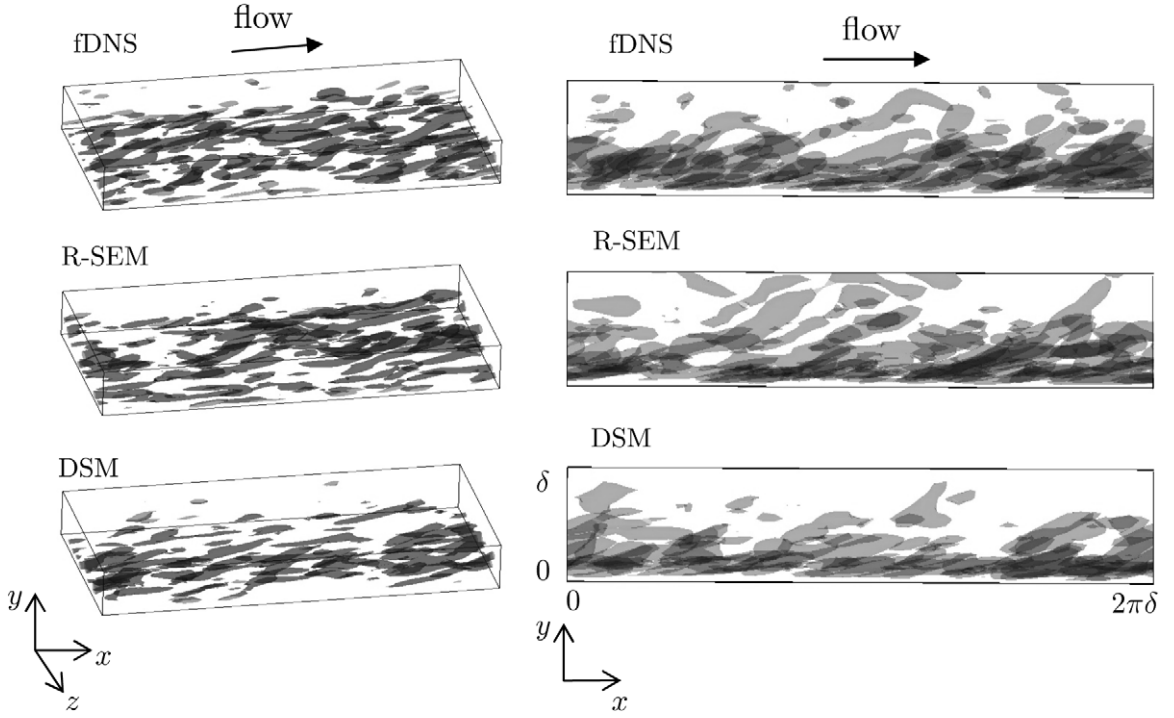

Fig. 7. Instantaneous vortical structures in turbulent channel flow at $Re_\tau = 180$ (Case I) visualized using positive Q criteria with $Q = 0.2u_\tau^4/\nu^2$. For xy-plane representation (right), all structures in the spanwise direction are superimposed with 50% transparency. For visual clarity, LES results are interpolated onto a 96^3 grid.

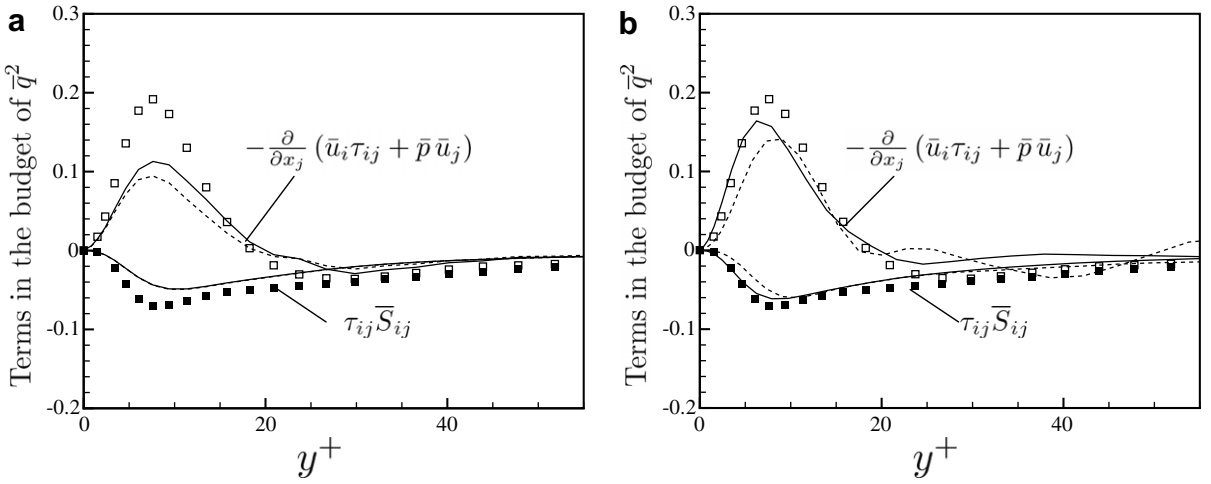

Fig. 8. SGS model contribution to the budget of resolved kinetic energy from (a) *a priori* test and (b) *a posteriori* test for turbulent channel flow at $Re_\tau = 180$ (Case I). □, $-\frac{\partial}{\partial x_j}(\bar{u}_i\tau_{ij} + \bar{p}\bar{u}_j)$ from DNS data; ■, $\tau_{ij}\overline{S}_{ij}$ from DNS data; ···, dynamic Smagorinsky model; —, RSEM-S.

the lift-off of near-wall vortical structures appears to be better predicted by RSEM, as shown in Fig. 7. Note that near-wall structures predicted by the dynamic Smagorinsky model are mostly confined to the near-wall region. These 'attached' vortical structures cause under-prediction of the wall-normal velocity spectra E_{vv} and over-prediction of the streamwise spectra E_{uu} (Fig. 6). The RSEM model predicts more realistic ejection motions and therefore more accurate E_{vv} and E_{uu}.

Why does the RSEM model yield better results than the dynamic Smagorinsky model in spite of being constrained by the same SGS dissipation? The interaction between the model and solution as in isotropic turbulence is one possibility. Another explanation is specific to inhomogeneous flows; SGS dissipation is not the only contribution of the SGS model to the resolved scale solution. For example, the resolved kinetic energy $\bar{q}^2 = \frac{1}{2}\bar{u}_i\bar{u}_i$, is governed by

$$\frac{\partial \bar{q}^2}{\partial t} = \frac{\partial}{\partial x_j}\left(-\bar{u}_j\bar{q}^2 - \bar{p}\bar{u}_j + \nu\frac{\partial \bar{q}^2}{\partial x_j}\right) - \nu\frac{\partial \bar{u}_i}{\partial x_j}\frac{\partial \bar{u}_i}{\partial x_j} - \frac{\partial}{\partial x_j}\left(\bar{u}_i\tau_{ij}\right) + \tau_{ij}\overline{S}_{ij}. \tag{19}$$

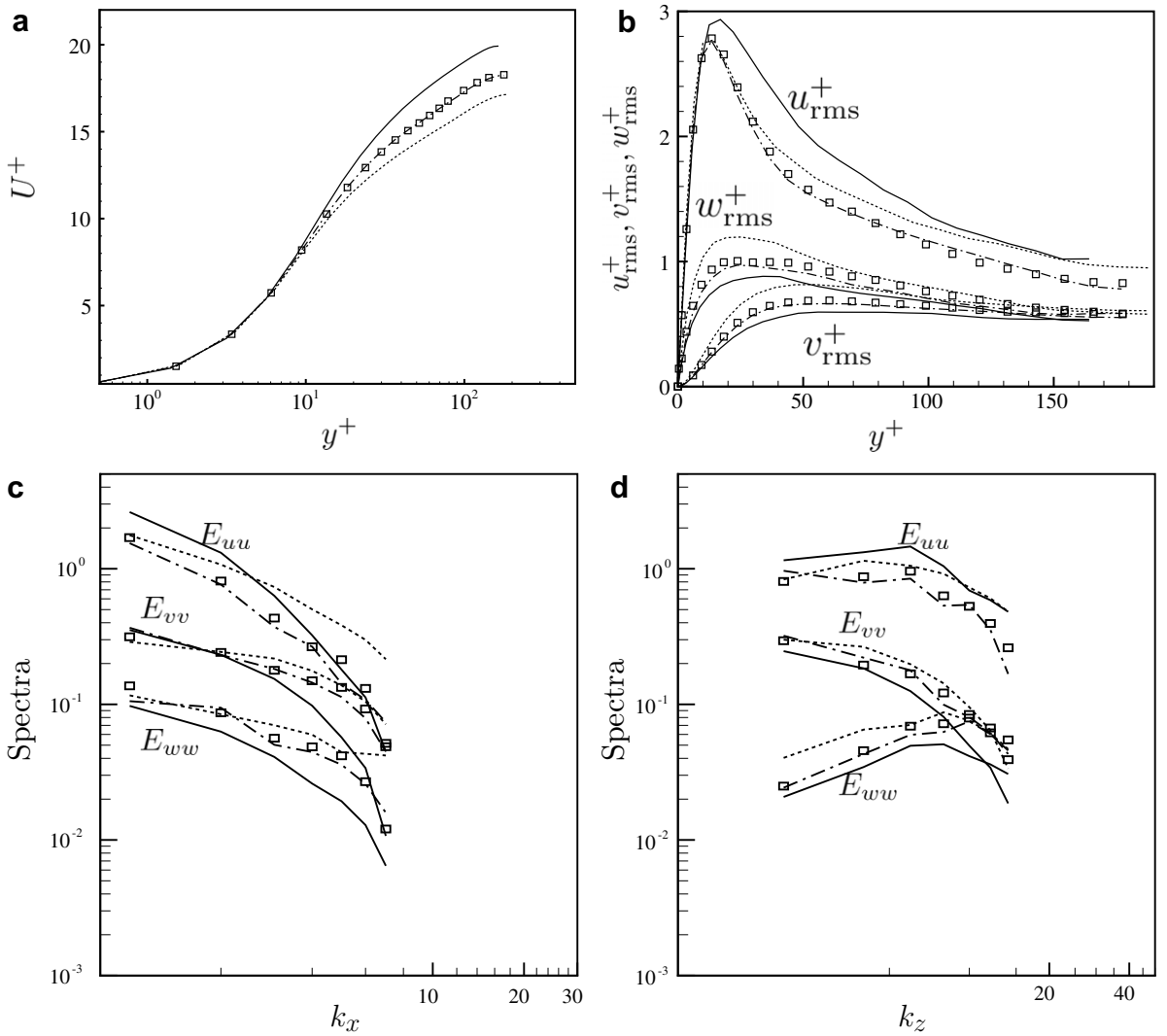

Fig. 9. Effects of RSEM formulation on turbulent channel flow at $Re_\tau = 180$: (a) mean streamwise velocity; (b) RMS velocity fluctuations; (c) streamwise and (d) spanwise velocity spectra at $y^+ = 30$. □, RSEM-S and matching the global dissipation; ----, RSEM-S and the least-square method; —, RSEM-D and matching the global dissipation; ···, RSEM-D and the least-square method.

Note that the SGS model affects resolved kinetic energy through the last two terms. The RSEM model is only constrained through SGS dissipation; the SGS diffusion term $-\frac{\partial}{\partial x_j}(\bar{u}_i\tau_{ij})$ is not constrained. Fig. 8 compares *a priori* and *a posteriori* computed SGS dissipation and diffusion terms for Case I between DNS data, LES with the dynamic Smagorinsky model and RSEM. Since the trace of SGS stress is not modeled but absorbed in the pressure for the dynamic Smagorinsky model, $-\frac{\partial}{\partial x_j}(\bar{u}_i\tau_{ij}+\bar{p}\bar{u}_j)$ (=SGS diffusion + pressure diffusion) terms are compared.

The comparison shown in Fig. 8 is interesting for many reasons. Note that the SGS diffusion term is larger than SGS dissipation in the near-wall region $y^+ < 20$. This implies that the SGS diffusion term plays an important role in the redistribution of kinetic energy, and therefore, in the dynamics of near-wall turbulence. Also, note the difference between predicted values of SGS dissipation from dynamic Smagorinsky model and RSEM. SGS diffusion from RSEM is closer to DNS data in the viscous sublayer as shown in Fig. 8(b). Note that even SGS dissipation predicted by *a posteriori* RSEM shows better agreement with DNS data in this region. It is also noteworthy that *a posteriori* results are in better agreement with DNS data while those from *a priori* test underpredict both SGS dissipation and diffusion.

4.2. Comparison between RSEM-S and RSEM-D

Estimation using the strain rate is contrasted to estimation using the deformation tensor in Figs. 9–11. For RSEM-D, two methods for coefficient determination are considered – matching the global dissipation (11), and the least-squares method (15). From Figs. 9 and 10, note that RSEM-D is highly sensitive to the coefficient determination method. As is evident from the velocity spectra (Fig. 9(c) and (d)), the results obtained using global dissipation are overly dissipative, as also observed for isotropic turbulence. The least-squares-based method shows insufficient dissipation, underpredicts the mean velocity and overpredicts spanwise and wall normal rms velocity fluctuations (Fig. 9). This sensitivity is not observed in the RSEM-S model; as shown in Fig. 9(a) and (b), mean velocity and RMS velocity fluctuation from RSEM-S with the least-squares method are very close to those obtained using global dissipation.

Fig. 11 shows the correlation of the dissipation predicted by RSEM-D with the dynamic Smagorinsky model (Fig. 11(a)), the p.d.f. of fluctuation SGS dissipation at $y^+ \approx 12$ (Fig. 11(b)), and mean SGS dissipation and diffusion (Fig. 11(c)). Note that SGS dissipation from RSEM-D shows very low correlation (<0.4) with that from the dynamic Smagorinsky model. In contrast, RSEM-S shows a correlation coefficient higher than 0.8 throughout the channel. This behavior is due to large backward dissipation in RSEM-D as shown in Fig. 11(b). Note that the contribution of mean velocity gradient is subtracted in computing SGS dissipation as in Ref. [31]. As a consequence, the net transfer at $y^+ = 12$ is backward. The overall predictions of RSEM-D

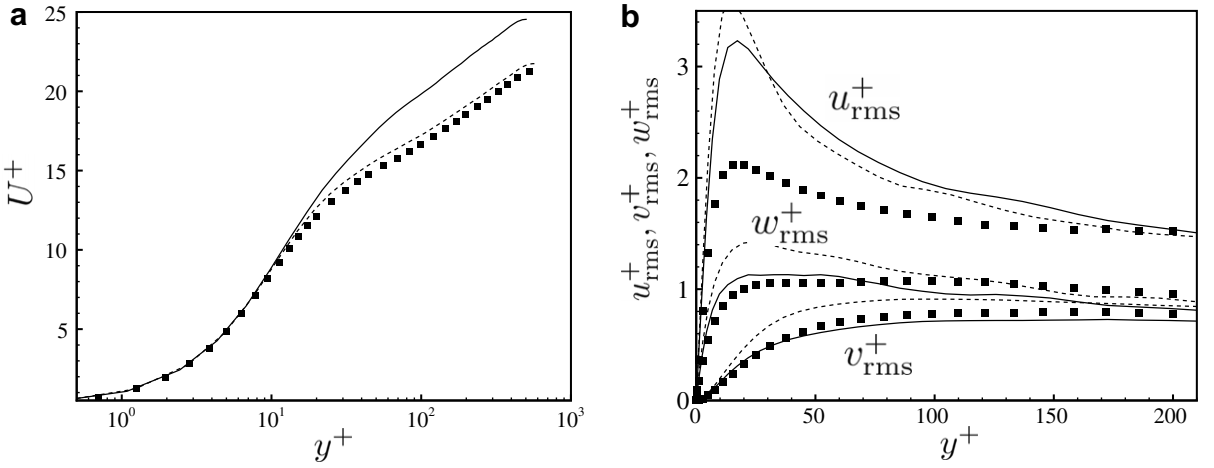

Fig. 10. Effects of RSEM formulation on turbulent channel flow at $Re_\tau = 590$ (Case III): (a) mean streamwise velocity; (b) RMS velocity fluctuations. ■, filtered DNS; ···, RSEM-D and matching the global dissipation; — RSEM-D and the least-square method.

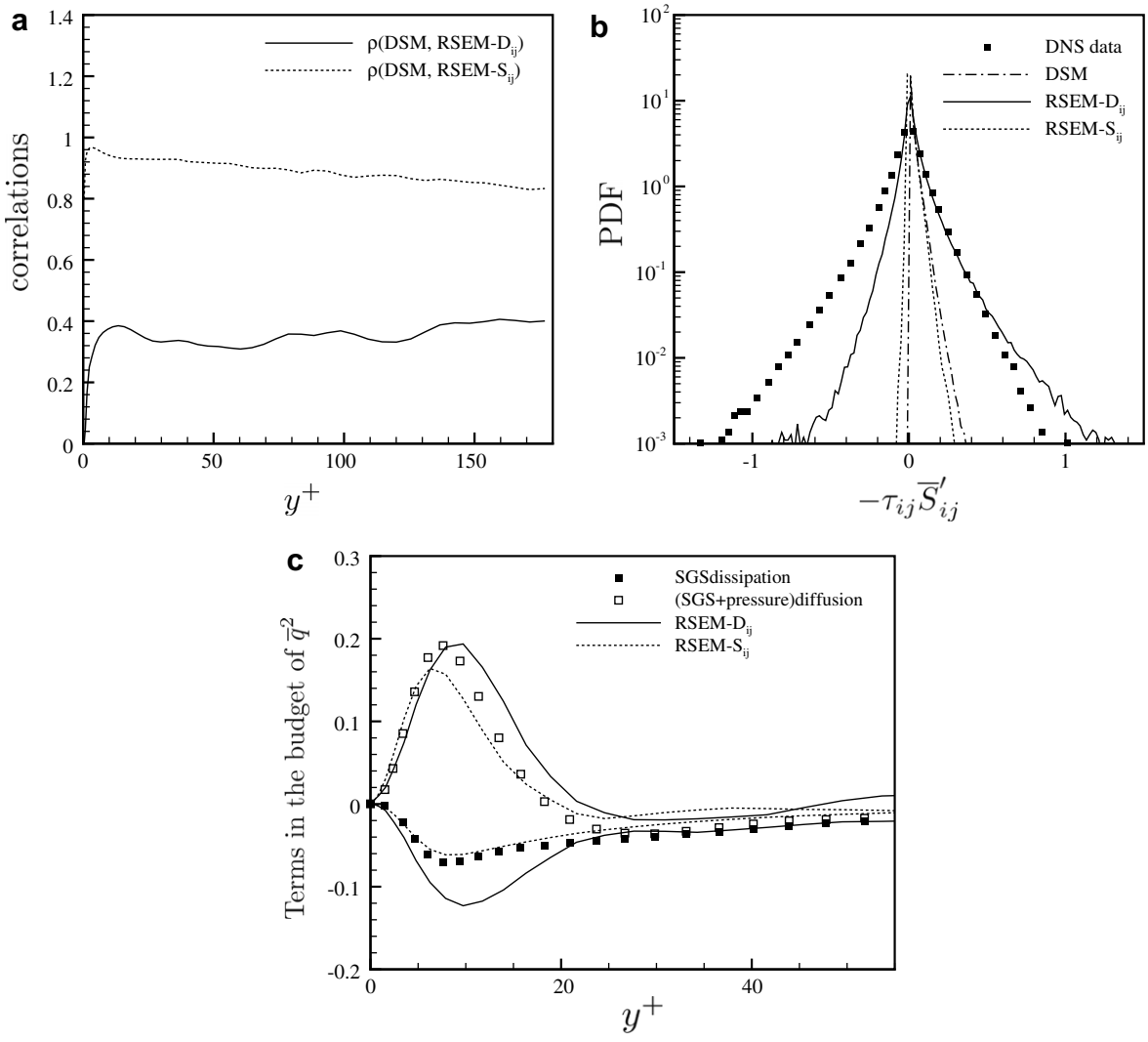

Fig. 11. Effects of RSEM formulations on turbulent channel flow at $Re_\tau = 180$: (a) correlations of SGS dissipation with dynamic Smagorinsky model; (b) PDF of fluctuation SGS dissipation (without mean velocity contribution) at $y^+ \approx 12$; (c) mean SGS dissipation and SGS diffusion. ···, RSEM-D; — RSEM-S; -·-·-, dynamic Smagorinsky model.

are not as good as RSEM-S; what is notable however, is (i) guaranteeing backscatter does not ensure better predictions, and (ii) the proposed modeling approach is stable even with large backscatter. From Fig. 11(c), it is interesting that RSEM-D yields less accurate prediction, not because it has large backward dissipation and low-correlation with DSM, but because the model predicts excessive SGS dissipation in the near-wall region where $y^+ < 20$.

5. Concluding remarks

This paper proposes a simple and effective modeling approach which incorporates the dissipative nature of existing eddy viscosity models into more physically appealing non-eddy viscosity SGS models. The key idea is use the SGS dissipation of the eddy viscosity model to constrain the coefficients of the non-eddy viscosity model. In order to demonstrate the feasibility of this approach, we propose a new, resolved subgrid scale estimation model (RSEM). The model is formulated directly on the LES grid, and SGS dissipation is guaranteed

by using a target SGS dissipation. The model has no adjustable coefficients, does not require finer grids, and can be easily applied to unstructured grids. Two versions of the model are considered, that differ in the use of strain rate (RSEM-S) or deformation tensor (RSEM-D) to estimate the velocity. Of these, the RSEM-S model is found superior.

The model is applied to decaying isotropic turbulence and turbulent channel flow and shown to yield promising results. For isotropic turbulence, RSEM predicts some level of backward dissipation, while yielding as excellent statistics as the dynamic Smagorinsky model. For channel flow, the results from RSEM are better than the dynamic Smagorinsky model, for both statistics and instantaneous flow structures. The strain-rate-based model (RSEM-S) results in the dominance of forward dissipation. The deformation-tensor based model (RSEM-D) has large backward dissipation and its dissipation distribution is more Gaussian. In spite of the large levels of backward dissipation, stable solutions are obtained.

In principle, the proposed idea of constraining SGS dissipation can be applied to any similarity type model to determine model coefficients. This is therefore an alternative to the Germano identity for determining model coefficients. Also, note that SGS dissipation is not necessarily the only constraint that can be imposed, although it is possibly the most important. SGS kinetic energy can be considered as another constraint, because having the SGS kinetic energy enables direct comparison of LES results to unfiltered experimental data. In this regard, note that the proposed RSEM model underestimates the normal components of SGS stress, and thus the SGS kinetic energy. Therefore, the comparison with unfiltered DNS data is not satisfactory for both isotropic turbulence, and channel flow. This behavior is most likely a limitation of only using SGS-dissipation as a constraint; no constraint on SGS kinetic energy can be imposed since $\tau_{ij}\overline{S}_{ij} = (\tau_{ij} - \frac{1}{3}\tau_{kk}\delta_{ij})\overline{S}_{ij}$. Extensions of the present formulation using the transport equation for $\overline{u}_i'$ or SGS kinetic energy, appear to be a promising direction for future development.

Acknowledgments

This work was supported by the Air Force Office of Scientific Research under grant FA9550-04-1-0341. Computer time was provided by the Minnesota Supercomputing Institute, the San Diego Supercomputer Center, and the National Center for Supercomputing Applications.

References

[1] S. Ghosal, An analysis of numerical errors in large-eddy simulations of turbulence, J. Comput. Phys. 125 (1996) 187.
[2] J. Gullbrand, F.T. Chow, The effect of numerical errors and turbulence models in large-eddy simulations of channel flow, with and without explicit filtering, J. Fluid Mech. 495 (2003) 323.
[3] M. Germano, U. Piomelli, P. Moin, W. Cabot, A dynamic subgrid-scale eddy viscosity model, Phys. Fluids A 3 (1991) 1760.
[4] U. Piomelli, W.H. Cabot, P. Moin, S. Lee, Subgrid-scale backscatter in turbulent and transitional flows, Phys. Fluids A 3 (1991) 1766.
[5] C. Meneveau, J. Katz, Scale-invariance and turbulence models for large-eddy simulation, Annu. Rev. Fluid Mech. 32 (2000) 1.
[6] C.B. da Silva, O. Metais, On the influence of coherent structures upon interscale interaction in turbulent plane jets, J. Fluid Mech. 473 (2002) 103.
[7] P. Sagaut, Large Eddy Simulation for Incompressible Flows, second ed., Springer, 2003.
[8] J. Bardina, J.H. Ferziger, W.C. Reynolds, Improved subgrid-scale models for large eddy simulation, AIAA Pap. 80-1357, 1980.
[9] S. Liu, C. Meneveau, J. Katz, On the properties of similarity subgrid-scale models and deduced from measurements in a turbulent jet, J. Fluid Mech. 275 (1994) 83.
[10] N. Park, J.Y. Yoo, H. Choi, Toward improved consistency of a priori tests with *a posteriori* tests in large eddy simulation, Phys. Fluids 17 (2005) 015103.
[11] J.A. Domaradzki, R.S. Rogallo, Local energy transfer and nonlocal interactions in homogeneous, isotropic turbulence, Phys. Fluids A 2 (1990) 413.
[12] J.A. Langford, R.D. Moser, Optimal LES formulations for isotropic turbulence, J. Fluid Mech. 398 (1999) 321.
[13] R. Akhavan, A. Ansari, S. Kang, N. Mangiavacchi, Subgrid-scale interactions in a numerically simulated planar turbulent jet and implications for modelling, J. Fluid Mech. 408 (2000) 83.
[14] Y. Zang, R.L. Street, J. Koseff, A dynamic mixed subgrid-scale model and it application to turbulent recirculating flows, Phys. Fluids A 5 (1993) 3186.
[15] B. Vreman, B. Geurts, H. Kuerten, Large eddy simulation of the turbulent mixing layer, J. Fluid Mech. 339 (1997) 357.
[16] R.C. Schmidt, A.R. Kerstein, S. Winsch, V. Nilsen, Near-wall LES closure based on one-dimensional turbulence modeling, J. Comput. Phys. 186 (2003) 317.
[17] K.A. Kemenov, S. Menon, Explicit small-scale velocity simulation for high-Re turbulent flows, J. Comput. Phys. 220 (2006) 290.

[18] J.A. Domaradzki, K.C. Loh, The subgrid-scale estimation model in the physical space representation, Phys. Fluids 11 (1999) 2330.
[19] J.A. Domaradzki, K.C. Loh, P.P. Yee, Large eddy simulations using the subgrid-scale estimation model and truncated Navier–Stokes dynamics, Theor. Comput. Fluid Dyn. 15 (2002) 421.
[20] G.C. Burton, J.A. Dahm, Multifractional subgrid-scale modeling for large-eddy simulation. II. Backscatter limiting and a posteriori evaluation, Phys. Fluids 17 (2005) 075112.
[21] A. Scotti, C. Meneveau, A fractal model for large eddy simulation of turbulent flow, Physica D 127 (1999) 198.
[22] C.G. Speziale, Galilean invariance of subgrid-scale stress model in the large-eddy simulation of turbulence, J. Fluid MecR-SEMh. 156 (1985) 55.
[23] F. Deutsch, Best Approximation in Inner Product Spaces, Springer-Verlag, New York, 2001.
[24] N. Park, J.Y. Yoo, H. Choi, Discretization errors in large eddy simulation: on the suitability of centered and upwind-biased compact difference schemes, J. Comput. Phys. 198 (2004) 580.
[25] G. Comte-Bellot, S. Corrsin, Simple Eulerian time correlation of full- and narrow-band velocity signals in grid-generated, 'isotropic' turbulence, J. Fluid Mech. 48 (1971) 273.
[26] N. Park, K. Mahesh, Analysis of numerical errors in large eddy simulation using statistical closure theory, J. Comput. Phys. 222 (2007) 194.
[27] N. Park, S. Lee, J. Lee, H. Choi, A dynamic subgrid-scale eddy viscosity model with a global model coefficient, Phys. Fluids 18 (2006) 125109.
[28] J. Kim, P. Moin, R.D. Moser, Turbulence statistics in fully developed channel flow at low Reynolds number, J. Fluid Mech. 177 (1987) 133.
[29] R.D. Moser, J. Kim, N.N. Mansour, DNS of turbulent channel flow up to $Re_\tau = 590$, Phys. Fluids 11 (1998) 943.
[30] Y. Dubief, F. Delcayre, On coherent vortex identification in turbulence, J. Turbul. 1 (2000).
[31] C. Härtel, L. Kleiser, Analysis and modelling of subgrid-scale motions in near-wall turbulence, J. Fluid Mech. 356 (1998) 327.